Published in final edited form as:

Anal Bioanal Chem. 2015 March ; 407(8): 2073–2084. doi:10.1007/s00216-014-8220-y.

Quantitative mass spectrometry imaging of emtricitabine in cervical tissue model using infrared matrix-assisted laser desorption electrospray ionization

Mark T. Bokhart,
W.M. Keck Fourier Transform Mass Spectrometry Laboratory, Department of Chemistry, North Carolina State University, Raleigh, NC 27695, USA

Elias Rosen,
W.M. Keck Fourier Transform Mass Spectrometry Laboratory, Department of Chemistry, North Carolina State University, Raleigh, NC 27695, USA

Corbin Thompson,
Eshelman School of Pharmacy, The University of North Carolina at Chapel Hill, Chapel Hill, NC 27599, USA

Craig Sykes,
Eshelman School of Pharmacy, The University of North Carolina at Chapel Hill, Chapel Hill, NC 27599, USA

Angela D. M. Kashuba, and
Eshelman School of Pharmacy, The University of North Carolina at Chapel Hill, Chapel Hill, NC 27599, USA

David C. Muddiman
W.M. Keck Fourier Transform Mass Spectrometry Laboratory, Department of Chemistry, North Carolina State University, Raleigh, NC 27695, USA

David C. Muddiman: david_muddiman@ncsu.edu

Abstract

A quantitative mass spectrometry imaging (QMSI) technique using infrared matrix-assisted laser desorption electrospray ionization (IR-MALDESI) is demonstrated for the antiretroviral (ARV) drug emtricitabine in incubated human cervical tissue. Method development of the QMSI technique leads to a gain in sensitivity and removal of interferences for several ARV drugs. Analyte response was significantly improved by a detailed evaluation of several cationization agents. Increased sensitivity and removal of an isobaric interference was demonstrated with sodium chloride in the electrospray solvent. Voxel-to-voxel variability was improved for the MSI experiments by normalizing analyte abundance to a uniformly applied compound with similar characteristics to the drug of interest. Finally, emtricitabine was quantified in tissue with a calibration curve generated from the stable isotope-labeled analog of emtricitabine followed by

Electronic supplementary material The online version of this article (doi:10.1007/s00216-014-8220-y) contains supplementary material, which is available to authorized users.

cross-validation using liquid chromatography tandem mass spectrometry (LC-MS/MS). The quantitative IR-MALDESI analysis proved to be reproducible with an emtricitabine concentration of 17.2±1.8 μg/g_{tissue}. This amount corresponds to the detection of 7 fmol/voxel in the IR-MALDESI QMSI experiment. Adjacent tissue slices were analyzed using LC-MS/MS which resulted in an emtricitabine concentration of 28.4±2.8 μg/g_{tissue}.

Keywords

Mass spectrometry imaging; IR-MALDESI; Absolute quantification; Drug distribution; HIV; Selected reaction monitoring

Introduction

Mass spectrometry imaging (MSI) data is generated by recording mass spectra and the corresponding spatial location [1]. Construction of ion heat maps creates a visual representation of a compound relating the observed ion abundance with its location. MSI is quickly becoming an invaluable tool in drug distribution studies [2–4]. The efficacy of a drug can be limited by the ability to reach its intended target; plasma concentrations of a drug are often used but may not accurately reflect the concentration of the drug at its site of action [5]. Thus, spatial distribution of a drug in tissue can provide vital information related to the efficacy of a drug. Moreover, the use of a MSI strategy can provide additional information about endogenous compounds and metabolites.

Simultaneous analysis of multiple species while retaining spatial specificity is a challenge for current quantitative methods. Selective reaction monitoring (SRM) assays using liquid chromatography tandem mass spectrometry (LC-MS/ MS) for quantification of pharmaceuticals are commonly used for pharmacokinetic analysis of drugs in plasma and tissues [6]. These methods typically require extraction of the analyte from a tissue homogenate and result in the loss of spatial information within a tissue or organ. Alternative approaches such as quantitative whole body autoradiography (QWBA) or positron emission tomography (PET) offer the ability to visualize drug distribution into tissues while providing quantitative information [4, 7, 8]. However, QWBA and PET require radiolabeled compounds which only give information about the radiolabel and are therefore not able to distinguish between the parent compound and its metabolites. Further, these quantitative imaging techniques incur significant experimental cost especially in the analysis of multiple analytes in multidrug therapies.

Although MSI has proven its utility to provide important spatial information of drugs in tissue, quantitative information in MSI has proven difficult to achieve. Matrix-assisted laser desorption ionization (MALDI) has been used extensively in qualitative MSI and with some success of quantification [1, 7, 9–37]. The recent advances in quantification using MSI were the subject of recent review [38]. Quantitative MALDI MSI has several limitations including the need for organic matrix deposition for ionization of analytes; the analysis is also typically performed under vacuum. Ambient ionization mass spectrometry allows tissues to be sampled at conditions much closer to their natural state [39].

Pixel-to-pixel variability in MSI poses the biggest challenge for quantification [40]. This variability can arise from a range of sources, including morphological features, ionization efficiency, and detection efficiency. Increasing sensitivity and reducing variability are essential steps toward making MSI a routine quantitative technique. Several groups have reported various normalization methods to account for tissue-specific signal response and reduced variation per pixel [18, 26, 27]. These studies exemplify the need for a suitable normalization compound to produce quantitative MSI data. The ideal normalization compound accounts for structure-specific ablation and ionization efficiency for the analyte. Stable isotope-labeled compounds are the best normalization compounds, as they are chemical and structural analogs of the target analyte.

Matrix-assisted laser desorption electrospray ionization (MALDESI) was first presented in 2006 using a UV laser to resonantly excite an organic matrix with secondary post ionization by electrospray ionization (ESI) [41]. Several other reports demonstrate the use of ESI for post ionization of a laser ablation plume [42, 43]. The use of a mid-infrared (IR) laser (2.94 μm) in MALDESI allows the use of endogenous and exogenous ice matrix to be used as a matrix, thus simplifying the sample preparation steps and providing spectra without matrix peak interference [44]. High fluence of the mid-IR laser allows IR-MALDESI to completely ablate through a 10 μm thick tissue section at each rastered position in two laser pulses, resulting in the analysis of a voxel of tissue [44]. Recently, the quantitative measurement abilities of the secondary ionization source laser electrospray mass spectrometry (LEMS) were reported for equimolar and nonequimolar solutions of multiple analytes [45]. LEMS was demonstrated to have a monotonic signal response as a function of concentration which was similar to ESI.

The need for a reliable method of characterizing spatial distribution of drug therapies within tissues, and the advantages of MSI, is exemplified within the field of human immunodeficiency virus (HIV). HIV replication has been shown to persist in certain anatomic sites such as the lymphatic system and reproductive tract [46, 47]. These viral reservoirs represent a significant obstacle in the cure of HIV. Evaluations of antiretroviral (ARV) penetration into these reservoirs are critical for understanding whether current therapies will be sufficient to completely eliminate HIV from the body. MSI represents a promising technique to advance the understanding of within-tissue ARV distribution and to provide invaluable information toward the development of drug therapies targeting the HIV reservoir.

Herein, we present a quantitative mass spectrometry imaging (QMSI) technique for the quantification of emtricitabine, a commonly used ARV [48], in human cervical tissue. Prior to quantification, several approaches for enhancing detection of multiple ARV drugs via IR-MALDESI MSI were evaluated. Tissue or morphologic specific ionization variability was then specifically addressed by using normalization compound-coated slides. Increased sensitivity and reduced voxel-to-voxel variability subsequently allowed for quantification of therapeutically relevant concentrations of emtricitabine in tissue by IR-MALDESI MSI. Cross-validation was performed using a validated LC-MS/MS method for adjacent tissue slices.

Experimental

Materials

HPLC grade methanol and water were purchased from Burdick and Jackson (Muskegon, MI, USA). Sodium chloride (>99.5 %), silver nitrate (>99 %), potassium chloride (>99.5 %), formic acid (LC/MS grade), lamivudine (>98 %), acyclovir (>99 %), and prednisolone (>99 %) were purchased from Sigma-Aldrich (St. Louis, MO, USA). Emtricitabine (FTC), tenofovir (TFV), and raltegravir (RAL) were obtained from the NIH AIDS Reagent Program, directed by the Pathogenesis and Basic Research Branch, Basic Sciences Program, Division of AIDS (DIADS), NIAID, NIH. $^{13}C^{15}N_2$-FTC and $^{13}C_5$-TFV were purchased from Moravek Biochemicals (Brea, CA, USA). The structures of the ARV drugs and prednisolone are shown in Fig. 1. All materials were used as received without further purification.

Tissue samples

Human cervical tissues were obtained from the University of North Carolina Tissue Procurement Facility through UNC IRB #09-0921. The tissues were prepared and incubated in FTC, TFV, and RAL at a concentration of 100 μg/mL as previously described [49]. Tissues were cryosectioned using a Leica CM1950 cryomicrotome (Buffalo Grove, IL, USA) to a thickness of 10 μm.

IR-MALDESI imaging

The imaging MALDESI source coupled to the Q Exactive mass spectrometer (Thermo Scientific, Bremen, Germany) has been previously described in greater detail [44, 49, 50]. Briefly, a tissue section was thaw mounted onto a microscope slide and placed on a XYZ-controlled Peltier stage. The enclosure surrounding the source was purged with nitrogen (MWSC, Raleigh, NC, USA) to less than 3 % relative humidity (RH) prior to the Peltier stage being cooled to −9 °C for approximately 10 min. The cooled stage and sample were then exposed to the ambient RH in the laboratory air to form a thin ice layer on the sample. After a sufficient amount of ice was deposited, the enclosure was purged with nitrogen to an approximate RH of 10 % to balance the rate of ice formation and sublimation. Two pulses at a repetition rate of 20 Hz from a mid-IR laser λ =2.94 μm (IR-Opolette 2371, Opotek, Carlsbad, CA, USA) were used to resonantly excite endogenous and exogenous water on the sample causing complete ablation of tissue material. The ablated material from the laser pulse is ejected normal to the surface where it interacts with an intersecting ESI plume. The neutral species generated in the laser ablation event partition into the charged electrospray droplets where they undergo secondary ionization in an ESI-like mechanism [41, 51]. The tissue ablation threshold of the laser is approximately 150 μm [52]. The laser was rastered across the sample at a spot-to-spot distance of 100 μm using an oversampling technique [44, 53]. The Q Exactive mass analyzer was fully integrated with IR-MALDESI source and synchronized to accumulate ions in the C-trap from both laser pulses prior to a single Orbitrap acquisition. The mass range was set to *m*/*z* 150–600, with the mass resolving power set to RP_{FWHM}=140,000 at *m*/*z* 200. High mass measurement accuracy (MMA) within 2 ppm was achieved using protonated and sodiated adducts of diisooctyl phthalate as two internal lock masses at *m*/*z* 391.28428 and 413.26623 [54].

Electrospray ionization cationization agents

The effects of several cationization agents were investigated using cervical tissue incubated in ARV drug solution. The incubated tissue was analyzed using 0.2 % formic acid or 30 μm solutions of sodium chloride, potassium chloride, or silver nitrate in 50:50 (*v*/*v*) methanol/water as electrospray solvents. Subsequently, 100 nL spots of 4 μg/mL $^{13}C^{15}N_2$-FTC, $^{13}C_5$-TFV, TFV, FTC, RAL, lamivudine (3TC), acyclovir (ACV), and PRED solution were pipetted on top of a blank cervical tissue. The analyte spots were analyzed in duplicate with electrospray solvents containing 0.2 % formic acid or 0, 10, 20, 30, 40, and 50 μm sodium chloride in 50:50 (*v*/*v*) methanol/water.

Sample preparation for quantitative MSI

An overview of the quantification workflow using IR-MALDESI MSI is presented in Fig. 2. For quantitative MSI, microscope slides were evenly coated with 3TC, ACV, and PRED using an automated pneumatic sprayer (TM Sprayer, LEAP Technologies, Carrboro, NC, USA). 3TC, ACV, and PRED were selected as internal standards based on their structural similarities to the ARV drugs (Fig. 1). The conditions used for evenly coating a microscope slide using the TM sprayer are summarized in the Electronic Supplementary Material, Table S1. Cryosectioned tissue slices were subsequently thaw mounted onto the coated slides. For absolute quantification, a dilution series of $^{13}C^{15}N_2$-FTC in 50:50 (*v*/*v*) methanol/water at concentrations of 0, 0.25, 0.5, 1, 2, 4, 6, and 8 μg/mL was pipetted on top of the tissue using a modified microliter syringe (Hamilton Company, Reno, NV, USA). One hundred nanoliters of each standard solution was used for each calibration spot which covered an area approximately 1 mm in diameter on tissue. The absolute quantification was performed with five replicates.

Data processing

For generating ion images, the Thermo Fisher RAW files were converted to a mzXML file using MSConvert software from Proteowizard [55]. Composite images containing data sets from multiple acquisitions were created by converting the RAW file to a mzXL file using MSConvert followed by conversion into an imzML file using imzML converter [56]. The individual imzML files were then merged into a single master imzML file containing the stacked images from multiple experiments. mzXML or imzML file format was loaded into and processed in MSiReader, an open source, vendor neutral imaging software [57]. Ion abundance maps were created with a bin width of 5 ppm. Centroid values for analytes used in determining MMA (Electronic Supplementary Material, Fig. S1) were obtained using RawMeat 2.1 (VAST Scientific, Cambridge, MA, USA).

Quantitative IR-MALDESI imaging

All observed FTC and $^{13}C^{15}N_2$-FTC ion abundances were normalized to the internal standard 3TC in MSiReader unless otherwise noted. The concentration of each calibration spot was calculated by dividing the total amount of $^{13}C^{15}N_2$-FTC in picograms by the corresponding spot area in square millimeters as determined in MSiReader. The resulting calibration points are given as a concentration in picograms per square millimeter. This method accounts for variability in spot size from manually spotting the standard on the

tissue. The concentration of each calibration point was plotted against the corresponding normalized average $^{13}C^{15}N_2$-FTC/3TC ion abundance ratio. The resulting calibration points were fitted with an unweighted linear regression. The average ratio of incubated FTC to 3TC over the entire tissue was calculated. The concentration of FTC in tissue was determined using the average normalized ion abundance and the $^{13}C^{15}N_2$-FTC linear regression equation. This value represents incubated FTC as a concentration in picograms per square millimeter. The FTC concentration was converted to microgram per gram tissue assuming a tissue density of 1 mg/mm^3 for comparison to LC-MS/MS results.

LC-MS/MS quantification

For each tissue slice analyzed by IR-MALDESI, an adjacent 10 μm thick tissue slice was homogenized and analyzed by a validated LC-MS/MS method as previously described [49]. LC-MS/MS calibration standards were prepared at 0.3, 0.6, 1.5, 6, 15, 30, 75, 150, 255, and 300 ng/mL with quality control (QC) samples at 0.9, 21, and 240 ng/mL. The tissue slices were homogenized and extracted with 1 mL of solvent; therefore, the final concentration in nanograms per milliliter was equivalent to nanogram per tissue slice. The tissue area of the adjacent section analyzed by MALDESI QMSI was used to calculate the FTC concentration as microgram per gram tissue, assuming a tissue density of 1 mg/mm^3. All calibration and QC samples were within 10 % of their nominal concentrations.

Results and discussion

Sensitivity enhancement and interference removal

A single incubated cervical tissue was analyzed in four quadrants to compare different cationization agents, namely formic acid, NaCl, KCl, and $AgNO_3$. We hypothesized that different cationization agents may increase the ionization efficiency and simultaneously reduce the variability between spectra. Moreover, the corresponding *m*/*z* shift associated with different cations can be particularly advantageous in instances where an isobaric interference overlaps with the $[M+H^+]^+$ analyte peak. Figure 3A shows the optical image of the incubated tissue with the cationization agent labeled. The corresponding ion maps of FTC, TFV, and RAL with each respective adduct for each quadrant are summarized in Fig. 3B–D. The sodium adduct of the three incubated drugs is detected with higher ion abundance and with less variability than any of the other cationization agents (Electronic Supplementary Material, Table S2). The largest gain in detected ion abundance is observed for the detection of RAL, with nearly an order of magnitude increase. The high affinity of RAL toward sodium cations is attributed to its molecular structure (Fig. 1). RAL is classified as an integrase inhibitor, all of which share two common structural features: a hydrophobic benzyl moiety and a chelating triad to bind to two Mg^{2+} ions [58]. RAL is suspected to chelate sodium ions in a similar manner since Na^+ and Mg^{2+} have a similar ionic radius. The formation of two Na^+ adducts was negligible at the concentrations studied here (data not shown). Based on the improved response across all ARVs, NaCl was doped into the electrospray solvent for all subsequent experiments.

To further optimize the cationization conditions, the concentration of the sodium chloride in the electrospray solvent was systematically varied from 0 to 50 μm in 10 μm increments

using a series of ARV calibration spots of the same concentration. In addition, two spots were analyzed with 0.2 % formic acid for comparison to the previously optimized conditions. Ion maps of the protonated and sodiated molecules of $^{13}C^{15}N_2$-FTC are shown in Fig. 4. The $[M+H^+]^+$ to $[M+ Na^+]^+$ ratio decreased with increasing concentration of NaCl in solution as expected from competing ionization. However, a maximum $[^{13}C^{15}N_2$-FTC $+Na^+]^+$ ion abundance occurred at 30 μm. This maximum at 30 μm NaCl was consistent for all compounds in the solution (data not shown). Figure 4 also highlights the removal of an isobaric interference from the analyte. The protonated form of stable isotope-labeled (SIL) FTC, $[^{13}C^{15}N_2$-FTC$+H^+]^+$, had an isobaric interference which makes identification and quantification at low concentrations difficult. In contrast, the sodium adduct of the compound was free from this interference. Based on these results, 30 μm NaCl in 50:50 methanol/water was used for the quantification of the incubated tissues.

Normalization strategy

The QMSI calibration curve presented (Fig. 7) used the stable isotope-labeled analog to quantify the analyte. In the present study, a different but structurally similar compound was used as an internal standard to account for voxel-to-voxel variation because the SIL-FTC is being used for quantification. Fortunately, several structural analogs mimicking a specific nucleotide have been synthesized for use in ARV therapy. 3TC and FTC are cytosine analogs, while ACV and TFV are guanosine and adenosine analogs, respectively. The analytes and their respective normalization compounds are shown in Fig. 1.

The incorporation of a structurally similar normalization compound allows for the normalization of analyte ion abundances on a per voxel basis. It is important to note that the laser in IR-MALDESI experiments completely ablates all tissue material from each location to ensure the same amount of material is sampled at each position in the oversampling method used. This complete ablation also allows the use of internal standard to be placed under the tissue in the analysis and still be effectively sampled. Variability between IR-MALDESI response to standards spotted above and below tissue has been demonstrated to be less than 17 % (Electronic Supplementary Material, Fig. S2). 3TC, ACV, and PRED were evenly sprayed on a microscope slide at approximately 90 fmol/voxel prior to thaw mounting a 10 μm thick incubated tissue section.

Figure 5 shows the ion maps used in the normalization strategy presented. Figure 5A shows the absolute ion abundance for the sodium adduct of the incubated FTC, while Fig. 5B depicts the absolute ion abundance for the sodium adduct of the normalization compound, 3TC. The normalized ion map in Fig. 5C is created by taking the ratio of analyte to normalization compound at each voxel. The inclusion of a normalization compound has been previously shown to account for tissue-specific analyte response in MSI [26–28].

The complete ablation of the sample at each position is a major advantage over MALDI-based MSI techniques where compounds placed below the tissue may be incorporated at a lesser extent due to extraction into the tissue and then into the organic matrix used in MALDI analyses. Similarly, compounds placed on top of the tissue may be incorporated to a greater extent than compounds within the tissue, representing a surface concentration and not an in-tissue concentration. The extraction of compounds into the organic matrix is seen

to be one of the biggest sources of variability in MALDI MSI analysis. IR-MALDESI proves to circumvent most of these issues with the complete ablation of tissue at each spatial location. Therefore, each pixel in the ion maps actually represents a volume element of tissue and should be referred to as a voxel.

This work here is performed on a single tissue type, cervical, which was assumed to be relatively homogeneous in composition. Also, the incubation method used in distributing the compound within the tissue is assumed to be homogeneous. Finally, the internal standard was evenly applied using an automatic pneumatic sprayer and assumed to be homogeneously distributed. These assumptions allow us to develop a normalization strategy in order to reduce signal variability across the entire tissue. A consistent detected abundance would be optimal. The use of sodium cationization along with normalization to an evenly incorporated internal standard was able to reduce the voxel %RSD for the entire tissue from 56 % for $[FTC+H^+]^+$ (Fig. 5B) to 32 % for $[FTC+ Na^+]^+/[3TC+Na^+]^+$ (Fig. 5C). Although RAL and PRED are not structurally related, normalization of RAL to PRED produces an image with reduced variability per voxel, indicating similar extraction and ionization efficiencies. The images generated for TFV and RAL using the absolute abundance and with the normalization to their internal standard applied are shown in Electronic Supplementary Material, Fig. S3.

Accounting for ionization efficiency per voxel

The normalization method presented in Fig. 5 shows a significant improvement in the observed analyte heat map and a corresponding reduction in voxel %RSD. The 30 μm NaCl electrospray solvent produces both $[M+H^+]^+$ and $[M+Na^+]^+$ ions (Fig. 4) through competing ionization mechanisms. Since we know the amount of material ablated at each voxel is consistent, we are able to compare the competing protonation and sodiation processes on a per spectrum basis in a single experiment. Figure 6A, B shows the absolute ion abundances associated with the sodiated and protonated adducts, respectively. The ion maps show localized areas of higher ion abundance commonly referred to as hot spots in the MALDI community. An interesting result occurs when the analyte ion abundance is normalized to the competing cationization of the normalization compound (Fig. 6C, D). The images are visibly more heterogeneous, a statement that is supported by the increased corresponding voxel %RSD values for the normalized heat maps. The resulting differences in the ion maps are the direct result of the competing ionization efficiencies of protonation and sodiation. If the analyte is normalized to the normalization compound having the same adduct, the voxel-to-voxel %RSD values are significantly improved. This result is independent of which ionization mechanism, protonation or sodiation, is applied to the analyte and internal standard. This is evidence demonstrating that the internal standard is truly accounting for ionization efficiency per spectrum (voxel), which is crucial to reducing variability that prevents per voxel quantification in MSI.

Quantification of emtricitabine using MALDESI QMSI

The calibration curves for the MSI experiment were generated using the SIL analog of the analyte. This method allows for correction of tissue-specific response by placing the calibration curve directly on the analyzed tissue. The use of SIL calibration spots also allows

a direct comparison of analyte to the calibration curve, avoiding the use of a standard addition calibration curve. The accuracy and sensitivity of a standard addition curve may be adversely affected by the high voxel-to-voxel variability in MSI.

Calibration spots were placed on top of the tissue using the SIL analog of FTC. To account for variations in spot size, the concentration of the standard per area was calculated for each calibration level separately. This was seen to effectively reduce variability due to the area of the calibration spots. The concentration was then plotted against the average ratio of SIL-FTC to 3TC to generate the calibration curves for the five QMSI replicates. Construction of interday calibration curves leads to differences in sensitivity as represented by variability in the slope of the calibration curve. This may be due to a variety of interday differences including the amount and composition of ambient ions, electrospray stability, or long-term stability of analyte and normalization compounds. Nonetheless, the average ratio of incubated FTC to internal standard 3TC of the entire tissue can be taken, related back to the SIL-FTC calibration curves generated to give a tissue average concentration in picograms per square millimeter. The total area of the tissue is known from the MSI analysis in MSiReader, which in conjunction with the calculated concentration can give the amount of FTC in the tissue slice. A representative calibration curve is shown in Fig. 7.

The average tissue concentration calculated from the calibration curves is given per 1 mm^2, which allows for the direct comparison of the five samples. The average FTC tissue concentration of 172.0±17.4 pg/mm^2 (±95 % CI, n=5) calculated from the IR-MALDESI QMSI analysis indicates good agreement between QMSI replicates. The total amount of drug in the tissue slice was calculated using the total area and its corresponding concentration. To allow comparison of QMSI to LC-MS/MS data for all replicates, the concentration of FTC was given as micrograms per gram tissue. The average FTC tissue concentration was 17.2 ± 1.8 $\mu g/g_{tissue}$ for IR-MALDESI QMSI data. Relative to LC-MS/MS, IR-MALDESI detection of FTC on a per voxel basis requires significantly higher sensitivity since the sample volume is greatly reduced. This spatial information provides important insight into the distribution of the compound but challenges instrument detection limits. The QMSI data presented represents the detection limit of the compound at approximately 7 fmol/voxel.

Comparison to LC-MS/MS

Ultimately, the IR-MALDESI QMSI experiment was cross-validated using a SRM LC-MS/MS assay on adjacent slices of the incubated tissue. The overall size of the tissue changed by approximately 20 % over the course of sectioning the irregularly shaped tissue. This change in tissue size can be correlated to a change in absolute amount of tissue analyzed and must be compensated for in the comparison of intra-LC-MS/MS analyses and the IR-MALDESI QMSI analyses. The average tissue FTC amount was 28.4±2.8 $\mu g/g_{tissue}$ based on LC-MS/MS data. Summary of the QMSI and LC-MS/MS results are presented in Table 1. FTC concentrations obtained from IR-MALDESI QMSI and LC-MS/MS analyses are in good agreement with each other; however, they are not within the error of either measurement. As previously discussed, IR-MALDESI completely ablates the entire volume of tissue present at a given ablation spot, such that the difference is not likely to be solely

attributable to a surface vs. volume concentration difference as often seen in MALDI MSI. Further work will be conducted to understand the source of any systematic error between these two methods.

Conclusion

A new approach for IR-MALDESI QMSI was demonstrated for the HIV drug FTC present in incubated cervical tissue. Sodium cationization was used to increase ion abundance and remove isobaric interference. A normalization compound was selected based on molecular structure and implemented during QMSI. Normalization led to reduced signal variability providing higher quality images and demonstrated improvements toward a per voxel quantification strategy. The total amount of FTC in tissue was 17.2±1.8 $\mu g/g_{tissue}$ for IR-MALDESI QMSI and 28.4±2.8 $\mu g/g_{tissue}$ based on LC-MS/MS data. The IR-MALDESI QMSI analyses represent the detection of FTC at approximately 7 fmol/voxel.

Supplementary Material

Refer to Web version on PubMed Central for supplementary material.

Acknowledgments

The authors gratefully acknowledge the financial support from the National Institutes of Health (R01GM087964), the W.M. Keck Foundation, and North Carolina State University.

References

1. Caprioli RM, Farmer TB, Gile J. Molecular imaging of biological samples: localization of peptides and proteins using MALDI-TOF MS. Anal Chem. 1997; 69:4751–4760. [PubMed: 9406525]
2. Prideaux B, Staab D, Stoeckli M. Applications of MALDI-MSI to pharmaceutical research. Methods Mol Biol. 2010; 656:405–413.10.1007/978-1-60761-746-4_23 [PubMed: 20680604]
3. Prideaux B, Stoeckli M. Mass spectrometry imaging for drug distribution studies. J Proteome. 2012; 75(16):4999–5013.10.1016/j.jprot.2012.07.028
4. Solon EG, Schweitzer A, Stoeckli M, Prideaux B. Autoradiography, MALDI-MS, and SIMS-MS imaging in pharmaceutical discovery and development. AAPS J. 2010; 12(1):11–26.10.1208/s12248-009-9158-4 [PubMed: 19921438]
5. Cohen MS, Gay C, Kashuba ADM, Blower S, Paxton L. Narrative review: antiretroviral therapy to prevent the sexual transmission of HIV-1. Ann Intern Med. 2007; 146(8):591–601.10.7326/0003-4819-146-8-200704170-00010 [PubMed: 17438318]
6. Xu RN, Fan L, Rieser MJ, El-Shourbagy TA. Recent advances in high-throughput quantitative bioanalysis by LC-MS/MS. J Pharm Biomed Anal. 2007; 44(2):342–355.10.1016/j.jpba.2007.02.006 [PubMed: 17360141]
7. Drexler DM, Tannehill-Gregg SH, Wang L, Brock BJ. Utility of quantitative whole-body autoradiography (QWBA) and imaging mass spectrometry (IMS) by matrix-assisted laser desorption/ ionization (MALDI) in the assessment of ocular distribution of drugs. J Pharmacol Toxicol Methods. 2011; 63(2):205–208.10.1016/j.vascn.2010.10.003 [PubMed: 21040797]
8. Rudin M, Weissleder R. Molecular imaging in drug discovery and development. Nat Rev Drug Discov. 2003; 2(2):123–131.10.1038/nrd1007 [PubMed: 12563303]
9. Barry JA, Groseclose MR, Robichaud G, Castellino S, Muddiman DC. Assessing drug and metabolite detection in liver tissue by UV-MALDI and IR-MALDESI mass spectrometry imaging coupled to FT-ICR MS. Int J Mass Spectrom. 201410.1016/j.ijms.2014.05.012

10. Bunch J, Clench MR, Richards DS. Determination of pharmaceutical compounds in skin by imaging matrix-assisted laser desorption/ionisation mass spectrometry. Rapid Commun Mass Spectrom. 2004; 18(24):3051–3060.10.1002/rcm.1725 [PubMed: 15543527]
11. Casadonte R, Caprioli RM. Proteomic analysis of formalin-fixed paraffin-embedded tissue by MALDI imaging mass spectrometry. Nat Protoc. 2011; 6(11):1695–1709.10.1038/nprot.2011.388 [PubMed: 22011652]
12. Djidja MC, Chang J, Hadjiprocopis A, Schmich F, Sinclair J, Mrsnik M, Schoof EM, Barker HE, Linding R, Jorgensen C, Erler JT. Identification of hypoxia-regulated proteins using MALDI-mass spectrometry imaging combined with quantitative proteomics. J Proteome Res. 201410.1021/pr401056c
13. Drexler DM, Garrett TJ, Cantone JL, Diters RW, Mitroka JG, Prieto Conaway MC, Adams SP, Yost RA, Sanders M. Utility of imaging mass spectrometry (IMS) by matrix-assisted laser desorption ionization (MALDI) on an ion trap mass spectrometer in the analysis of drugs and metabolites in biological tissues. J Pharmacol Toxicol Methods. 2007; 55(3):279–288.10.1016/j.vascn.2006.11.004 [PubMed: 17222568]
14. Fehniger TE, Vegvari A, Rezeli M, Prikk K, Ross P, Dahlback M, Edula G, Sepper R, Marko-Varga G. Direct demonstration of tissue uptake of an inhaled drug: proof-of-principle study using matrix-assisted laser desorption ionization mass spectrometry imaging. Anal Chem. 2011; 83(21):8329–8336.10.1021/ac2014349 [PubMed: 21942412]
15. Goodwin RJ, Mackay CL, Nilsson A, Harrison DJ, Farde L, Andren PE, Iverson SL. Qualitative and quantitative MALDI imaging of the positron emission tomography ligands raclopride (a D2 dopamine antagonist) and SCH 23390 (a D1 dopamine antagonist) in rat brain tissue sections using a solvent-free dry matrix application method. Anal Chem. 2011; 83(24):9694–9701.10.1021/ac202630t [PubMed: 22077717]
16. Goto T, Terada N, Inoue T, Nakayama K, Okada Y, Yoshikawa T, Miyazaki Y, Uegaki M, Sumiyoshi S, Kobayashi T, Kamba T, Yoshimura K, Ogawa O. The expression profile of phosphatidylinositol in high spatial resolution imaging mass spectrometry as a potential biomarker for prostate cancer. PLoS One. 2014; 9(2):e90242.10.1371/journal.pone.0090242 [PubMed: 24587297]
17. Groseclose MR, Castellino S. A mimetic tissue model for the quantification of drug distributions by MALDI imaging mass spectrometry. Anal Chem. 2013; 85(21):10099–10106.10.1021/ac400892z [PubMed: 24024735]
18. Hamm G, Bonnel D, Legouffe R, Pamelard F, Delbos JM, Bouzom F, Stauber J. Quantitative mass spectrometry imaging of propranolol and olanzapine using tissue extinction calculation as normalization factor. J Proteome. 2012; 75(16):4952–4961.10.1016/j.jprot.2012.07.035
19. Handberg E, Chingin K, Wang N, Dai X, Chen H. Mass spectrometry imaging for visualizing organic analytes in food. Mass Spectrom Rev. 201410.1002/mas.21424
20. Hsieh Y, Casale R, Fukuda E, Chen J, Knemeyer I, Wingate J, Morrison R, Korfmacher W. Matrix-assisted laser desorption/ionization imaging mass spectrometry for direct measurement of clozapine in rat brain tissue. Rapid Commun Mass Spectrom. 2006; 20(6):965–972.10.1002/rcm.2397 [PubMed: 16470674]
21. Hsieh Y, Chen J, Korfmacher WA. Mapping pharmaceuticals in tissues using MALDI imaging mass spectrometry. J Pharmacol Toxicol Methods. 2007; 55(2):193–200.10.1016/j.vascn.2006.06.004 [PubMed: 16919485]
22. Koeniger SL, Talaty N, Luo Y, Ready D, Voorbach M, Seifert T, Cepa S, Fagerland JA, Bouska J, Buck W, Johnson RW, Spanton S. A quantitation method for mass spectrometry imaging. Rapid Commun Mass Spectrom. 2011; 25(4):503–510.10.1002/rcm.4891 [PubMed: 21259359]
23. Kubo A, Kajimura M, Suematsu M. Matrix-assisted laser desorption/ionization (MALDI) imaging mass spectrometry (IMS): a challenge for reliable quantitative analyses. Mass Spectrom (Tokyo). 2012; 1(1):A0004.10.5702/massspectrometry.A0004 [PubMed: 24349905]
24. Lietz CB, Gemperline E, Li LJ. Qualitative and quantitative mass spectrometry imaging of drugs and metabolites. Adv Drug Deliv Rev. 2013; 65(8):1074–1085.10.1016/j.addr.2013.04.009 [PubMed: 23603211]
25. Nilsson A, Fehniger TE, Gustavsson L, Andersson M, Kenne K, Marko-Varga G, Andren PE. Fine mapping the spatial distribution and concentration of unlabeled drugs within tissue

microcompartments using imaging mass spectrometry. PLoS One. 2010; 5(7):e11411.10.1371/journal.pone.0011411 [PubMed: 20644728]

26. Pirman DA, Kiss A, Heeren RM, Yost RA. Identifying tissue-specific signal variation in MALDI mass spectrometric imaging by use of an internal standard. Anal Chem. 2013; 85(2):1090–1096.10.1021/ac3029618 [PubMed: 23214468]
27. Pirman DA, Reich RF, Kiss A, Heeren RM, Yost RA. Quantitative MALDI tandem mass spectrometric imaging of cocaine from brain tissue with a deuterated internal standard. Anal Chem. 2013; 85(2):1081–1089.10.1021/ac302960j [PubMed: 23214490]
28. Pirman DA, Yost RA. Quantitative tandem mass spectrometric imaging of endogenous acetyl-L-carnitine from piglet brain tissue using an internal standard. Anal Chem. 2011; 83(22):8575–8581.10.1021/ac201949b [PubMed: 21942933]
29. Prideaux B, Dartois V, Staab D, Weiner DM, Goh A, Via LE, Barry CE 3rd, Stoeckli M. High-sensitivity MALDI-MRM-MS imaging of moxifloxacin distribution in tuberculosis-infected rabbit lungs and granulomatous lesions. Anal Chem. 2011; 83(6):2112–2118.10.1021/ac1029049 [PubMed: 21332183]
30. Shin YG, Dong T, Chou B, Menghrajani K. Determination of loperamide in mdr1a/1b knock-out mouse brain tissue using matrix-assisted laser desorption/ionization mass spectrometry and comparison with quantitative electrospray-triple quadrupole mass spectrometry analysis. Arch Pharm Res. 2011; 34(11):1983–1988.10.1007/s12272-011-1119-7 [PubMed: 22139698]
31. Signor L, Varesio E, Staack RF, Starke V, Richter WF, Hopfgartner G. Analysis of erlotinib and its metabolites in rat tissue sections by MALDI quadrupole time-of-flight mass spectrometry. J Mass Spectrom. 2007; 42(7):900–909.10.1002/jms.1225 [PubMed: 17534860]
32. Stoeckli M, Staab D, Schweitzer A. Compound and metabolite distribution measured by MALDI mass spectrometric imaging in whole-body tissue sections. Int J Mass Spectrom. 2007; 260(2–3):195–202.10.1016/j.ijms.2006.10.007
33. Sugiura Y, Konishi Y, Zaima N, Kajihara S, Nakanishi H, Taguchi R, Setou M. Visualization of the cell-selective distribution of PUFA-containing phosphatidylcholines in mouse brain by imaging mass spectrometry. J Lipid Res. 2009; 50(9):1776–1788.10.1194/jlr.M900047-JLR200 [PubMed: 19417221]
34. Sun N, Walch A. Qualitative and quantitative mass spectrometry imaging of drugs and metabolites in tissue at therapeutic levels. Histochem Cell Biol. 2013; 140(2):93–104.10.1007/s00418-013-1127-4 [PubMed: 23881163]
35. Takai N, Tanaka Y, Inazawa K, Saji H. Quantitative analysis of pharmaceutical drug distribution in multiple organs by imaging mass spectrometry. Rapid Commun Mass Spectrom. 2012; 26(13):1549–1556.10.1002/rcm.6256 [PubMed: 22638972]
36. Trede D, Schiffler S, Becker M, Wirtz S, Steinhorst K, Strehlow J, Aichler M, Kobarg JH, Oetjen J, Dyatlov A, Heldmann S, Walch A, Thiele H, Maass P, Alexandrov T. Exploring three-dimensional matrix-assisted laser desorption/ionization imaging mass spectrometry data: three-dimensional spatial segmentation of mouse kidney. Anal Chem. 2012; 84(14):6079–6087.10.1021/ac300673y [PubMed: 22720760]
37. Velickovi XD, Ropartz D, Guillon F, Saulnier L, Rogniaux H. New insights into the structural and spatial variability of cell-wall polysaccharides during wheat grain development, as revealed through MALDI mass spectrometry imaging. J Exp Bot. 201410.1093/jxb/eru065
38. Ellis SR, Bruinen AL, Heeren RM. A critical evaluation of the current state-of-the-art in quantitative imaging mass spectrometry. Anal Bioanal Chem. 2014; 406(5):1275–1289.10.1007/s00216-013-7478-9 [PubMed: 24281323]
39. Nemes P, Vertes A. Ambient mass spectrometry for in vivo local analysis and in situ molecular tissue imaging. TrAC Trends Anal Chem. 2012; 34:22–34.10.1016/j.trac.2011.11.006
40. Cohen LH, Gusev AI. Small molecule analysis by MALDI mass spectrometry. Anal Bioanal Chem. 2002; 373(7):571–586.10.1007/s00216-002-1321-z [PubMed: 12219737]
41. Sampson JS, Hawkridge AM, Muddiman DC. Generation and detection of multiply-charged peptides and proteins by matrix-assisted laser desorption electrospray ionization (MALDESI) Fourier transform ion cyclotron resonance mass spectrometry. J Am Soc Mass Spectrom. 2006; 17(12):1712–1716.10.1016/j.jasms.2006.08.003 [PubMed: 16952462]

42. Nemes P, Vertes A. Laser ablation electrospray ionization for atmospheric pressure, in vivo, and imaging mass spectrometry. Anal Chem. 2007; 79:8098–8106. [PubMed: 17900146]
43. Brady JJ, Judge EJ, Levis RJ. Mass spectrometry of intact neutral macromolecules using intense non-resonant femtosecond laser vaporization with electrospray post-ionization. Rapid Commun Mass Spectrom. 2009; 23(19):3151–3157.10.1002/rcm.4226 [PubMed: 19714710]
44. Robichaud G, Barry JA, Muddiman DC. IR-MALDESI mass spectrometry imaging of biological tissue sections using ice as a matrix. J Am Soc Mass Spectrom. 2014; 25(3):319–328.10.1007/s13361-013-0787-6 [PubMed: 24385399]
45. Flanigan PM, Perez JJ, Karki S, Levis RJ. Quantitative measurements of small molecule mixtures using laser electrospray mass spectrometry. Anal Chem. 2013; 85(7):3629–3637.10.1021/ac303443q [PubMed: 23452308]
46. Chun TW, Nickle DC, Justement JS, Meyers JH, Roby G, Hallahan CW, Kottilil S, Moir S, Mican JM, Mullins JI, Ward DJ, Kovacs JA, Mannon PJ, Fauci AS. Persistence of HIV in gut-associated lymphoid tissue despite long-term antiretroviral therapy. J Infect Dis. 2008; 197(5):714–720.10.1086/527324 [PubMed: 18260759]
47. Launay O, Tod M, Tschope I, Si-Mohamed A, Belarbi L, Charpentier C, Goujard C, Taburet A-M, Lortholary O, Leroy V, Belec L. Residual HIV-1 RNA and HIV-1 DNA production in the genital tract reservoir of women treated with HAART: the prospective ANRS EP24 GYNODYN study. : 2040–2058. (electronic)).
48. <////Guidelines for the use of antiretroviral agents in HIV-1 infected adults and adolescents.pdf>
49. Barry JA, Robichaud G, Bokhart MT, Thompson C, Sykes C, Kashuba AD, Muddiman DC. Mapping antiretroviral drugs in tissue by IR-MALDESI MSI coupled to the Q exactive and comparison with LC-MS/MS SRM assay. J Am Soc Mass Spectrom. 201410.1007/s13361-014-0884-1
50. Barry JA, Muddiman DC. Global optimization of the infrared matrix-assisted laser desorption electrospray ionization (IR MALDESI) source for mass spectrometry using statistical design of experiments. Rapid Commun Mass Spectrom. 2011; 25(23):3527–3536.10.1002/rcm.5262 [PubMed: 22095501]
51. Sampson JS, Hawkridge AM, Muddiman DC. Development and characterization of an ionization technique for analysis of biological macromolecules: liquid matrix-assisted laser desorption electrospray ionization. Anal Chem. 2008; 80:6773–6778. [PubMed: 18656949]
52. Robichaud G, Barry JA, Garrard KP, Muddiman DC. Infrared matrix-assisted laser desorption electrospray ionization (IR-MALDESI) imaging source coupled to a FT-ICR mass spectrometer. J Am Soc Mass Spectrom. 2013; 24(1):92–100.10.1007/s13361-012-0505-9 [PubMed: 23208743]
53. Jurchen JC, Rubakhin SS, Sweedler JV. MALDI-MS imaging of features smaller than the size of the laser beam. J Am Soc Mass Spectrom. 2005; 16(10):1654–1659.10.1016/j.jasms.2005.06.006 [PubMed: 16095912]
54. Olsen JV, Godoy LMF, Li G, Macek B, Mortensen P, Pesch R, Makarov A, Lange O, Horning S, Mann M. Parts per million mass accuracy on an Orbitrap mass spectrometer via lock mass injection into a C-trap. Mol Cell Proteomics. 2005; 4:2010–2021. [PubMed: 16249172]
55. Kessner D, Chambers M, Burke R, Agus D, Mallick P. ProteoWizard: open source software for rapid proteomics tools development. Bioinformatics. 2008; 24(21):2534–2536.10.1093/bioinformatics/btn323 [PubMed: 18606607]
56. Schramm T, Hester A, Klinkert I, Both JP, Heeren RM, Brunelle A, Laprevote O, Desbenoit N, Robbe MF, Stoeckli M, Spengler B, Rompp A. imzML—a common data format for the flexible exchange and processing of mass spectrometry imaging data. J Proteome. 2012; 75(16):5106–5110.10.1016/j.jprot.2012.07.026
57. Robichaud G, Garrard KP, Barry JA, Muddiman DC. MSiReader: an open-source interface to view and analyze high resolving power MS imaging files on Matlab platform. J Am Soc Mass Spectrom. 2013; 24(5):718–721.10.1007/s13361-013-0607-z [PubMed: 23536269]
58. Wang Z, Tang J, Salomon CE, Dreis CD, Vince R. Pharmacophore and structure-activity relationships of integrase inhibition within a dual inhibitor scaffold of HIV reverse transcriptase and integrase. Bioorg Med Chem. 2010; 18(12):4202–4211.10.1016/j.bmc.2010.05.004 [PubMed: 20576573]

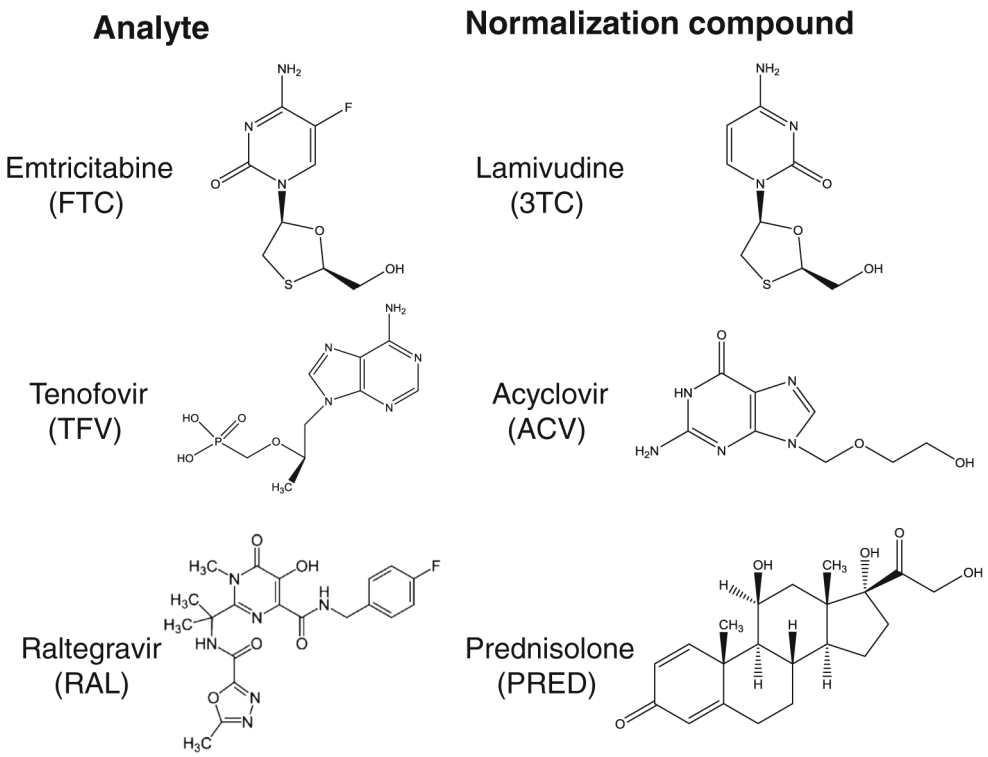

Fig. 1.

Structures of the targeted analytes. Emtricitabine (*FTC*) and lamivudine (*3TC*) are nucleoside reverse transcriptase inhibitors (*NRTIs*) and are cytosine analogs. Tenofovir (*TFV*) and acyclovir (*ACV*) are also NRTIs and are adenosine and guanosine analogs, respectively. Raltegravir (*RAL*) belongs to the HIV integrase inhibitor class of ARV drugs. Although not structurally similar, prednisolone (*PRED*) was used as an internal standard for RAL

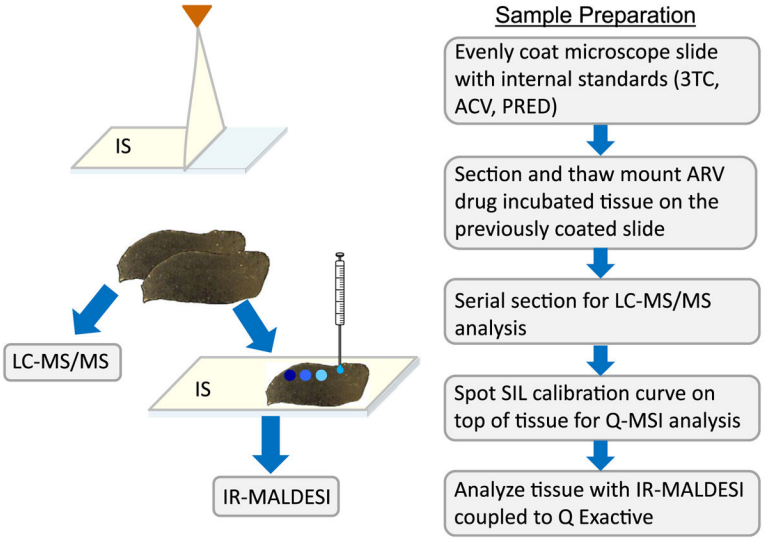

Fig. 2.
Workflow for quantitative IR-MALDESI MSI

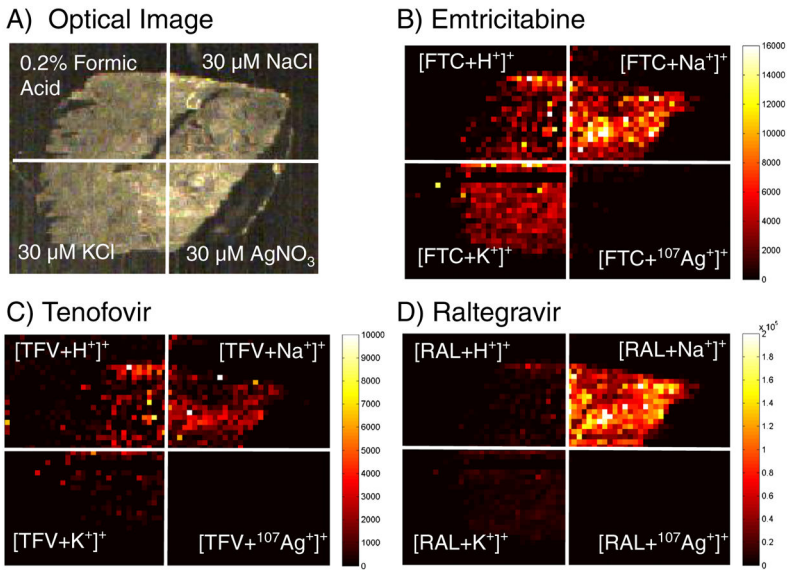

Fig. 3.

Cervical tissue incubated in 100 μg/mL ARV drug solution was analyzed using 0.2 % formic acid $[M+H^+]^+$, 30 μm sodium chloride $[M+ Na^+]^+$, 30 μm potassium chloride $[M+K^+]^+$, or 30 μm silver nitrate $[M+^{107}Ag^+]^+$ in 50:50 methanol water ESI solution. (**A**) Optical image of the tissue before exogenous ice matrix formation and ion maps for incubated (**B**) emtricitabine, (**C**) tenofovir, and (**D**) raltegravir

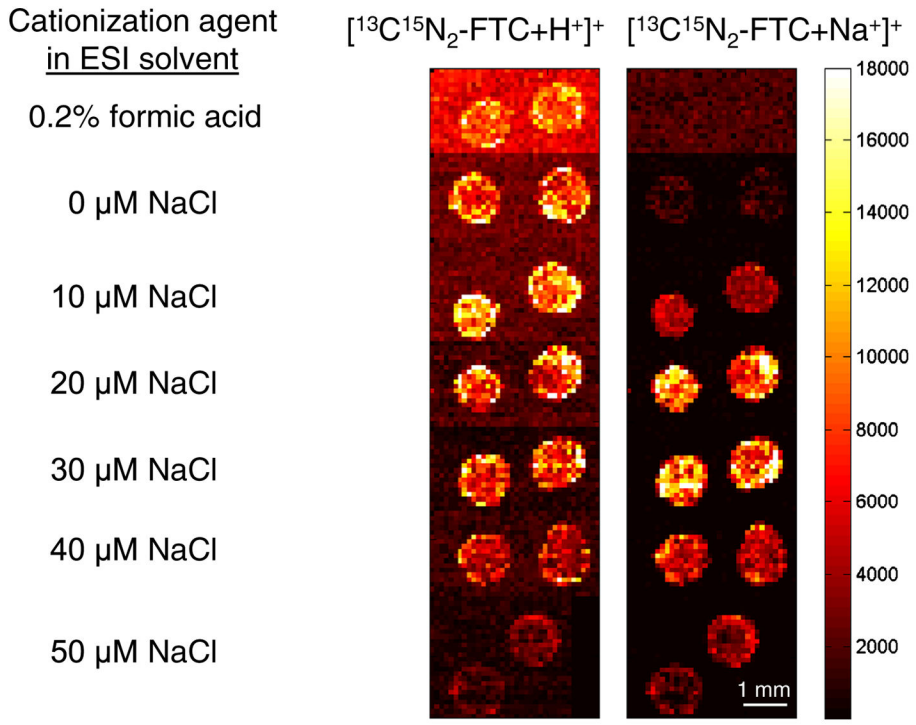

Fig. 4.

Composite image demonstrating the ionization effects of several concentrations of sodium chloride and 0.2 % formic acid in the ESI solvent. A solution containing all the ARV in the study was pipetted onto a blank tissue to determine optimum selectivity and sensitivity. The ion map of $^{13}C^{15}N_2$-FTC is shown to exemplify the use of 30 μm sodium chloride in the ESI solvent to remove isobaric interference and increase sensitivity

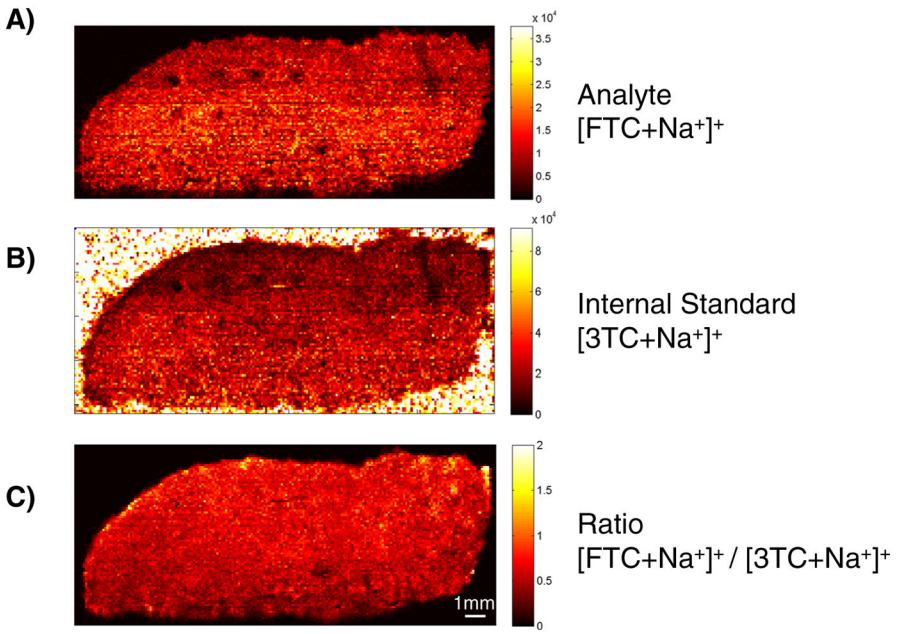

Fig. 5.

Visualization of the normalization process used to reduce variability at a per voxel basis of tissue replicate 2. Ion maps of (**A**) the absolute ion abundance of analyte $[FTC+ Na^+]^+$, (**B**) absolute ion abundance of normalization compound $[3TC+Na^+]^+$, (**C**) ratio of analyte to internal standard $[FTC+Na^+]^+/[3TC+Na^+]^+$

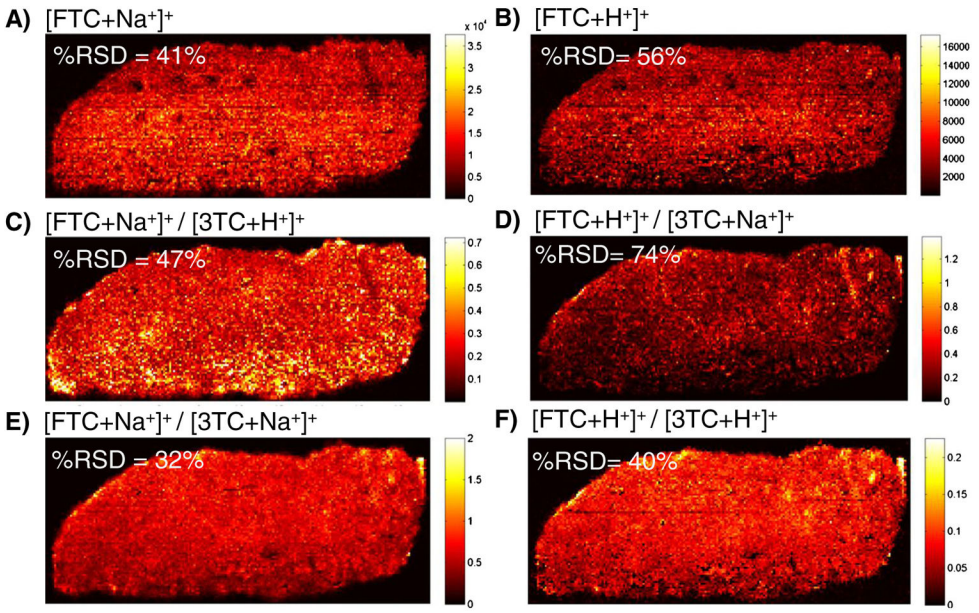

Fig. 6.

Ion maps comparing the ionization efficiencies of protonation and sodiation adducts of FTC. The ion map and %RSD for the entire tissue are shown for (**A**) $[FTC+Na^+]^+$ and (**B**) $[FTC+H^+]^+$ representing the detected ion abundance of FTC. The normalization of FTC to the competing ionization mechanism of internal standard for (**C**) $[FTC+Na^+]^+/[3TC+H^+]^+$ and (**D**) $[FTC+H^+]^+/[3TC+Na^+]^+$. The %RSD per pixel increases in both cross normalizations and the ion maps are visually more heterogeneous. Normalization of the analyte and internal standard with the same adduct produces the lowest pixel %RSD and improved visual quality for both the (**E**) sodiated and (**F**) protonated adducts

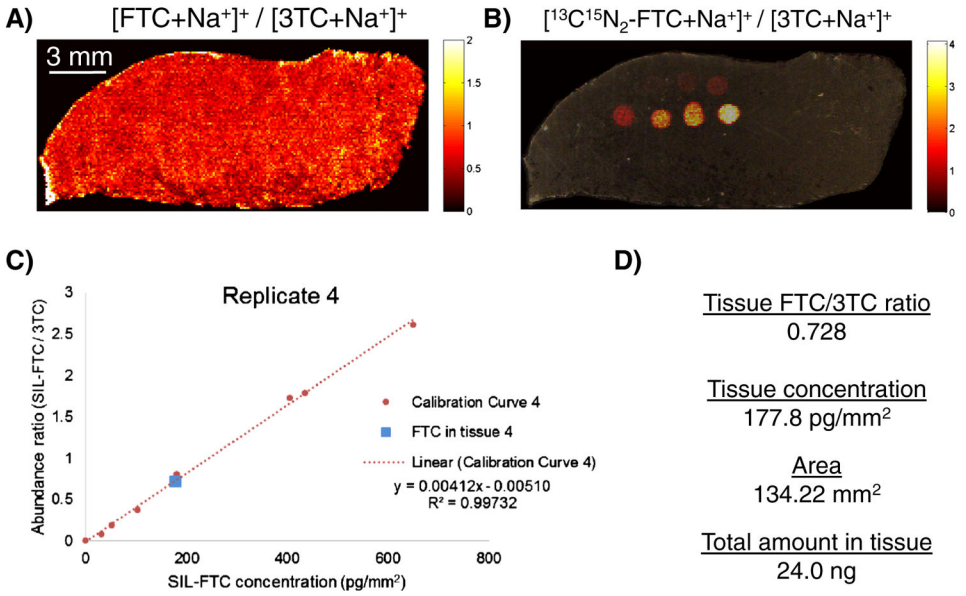

Fig. 7.

Summary of FTC quantification of tissue section 4. (**A**) Ion map of $[FTC+Na^+]^+/[3TC+Na^+]^+$ representing abundance of incubated FTC in the tissue section. The average ratio was 0.728. (**B**) Ion map of $[^{13}C^{15}N_2\text{-}FTC+Na^+]^+/[3TC+Na^+]^+$ representing the calibration curve at 0, 0.25, 0.5, 1, 2, 4, 6, and 8 μg/mL solution. (**C**) Resulting calibration curve generated from $^{13}C^{15}N_2$-FTC showing good linearity with R^2= 0.9973. The calculated tissue concentration was near the center of the calibration range. (**D**) Summary of values used to generate the total amount of drug present in tissue section. Using the average ratio and the equation of the calibration curve returns a value of the FTC concentration in tissue in picograms per square millimeter. Using the area of the tissue, the total amount of FTC in the section was determined to be 24.0 ng

Table 1

Quantification summary of the five tissue sections and the respective adjacent section analyzed by LC-MS/MS

	Replicate	**1**	**2**	**3**	**4**	**5**	**Average±95 % CI (μg/g$_{tissue}$)**
	Tissue area (mm^2)	**110.85**	**122.15**	**128.33**	**134.22**	**134.83**	
MALDESI	R^2	0.995	0.9978	0.9973	0.9973	0.9994	**17.2±1.8**
	pg/mm^2	171.4	148.0	179.4	177.8	184.2	
	μg/g$_{tissue}$	17.1	14.8	17.9	17.8	18.4	
LC-MS/MS	FTC (ng/tissue)	28.7	37.0	36.5	41.6	35.8	**28.4±2.8**
	μg/g$_{tissue}$	25.9	30.3	28.4	31.0	26.6	

Total amount of FTC in section is normalized to the largest tissue. The size of adjacent tissues analyzed by LC-MS/MS is assumed to be the same size as its MALDESI counterpart. For quantitative MALDESI MSI, the average concentration of FTC per tissue was found to be 17.2±1.8 μg/g$_{tissue}$ at the 95 % confidence interval. LC-MS/MS of adjacent sections had an average concentration of FTC of 28.4±2.8 μg/g$_{tissue}$